Beam Emission spectroscopy with radially and poloidally elongated optical sightlines [a)]

M.Ono[1,b)], K.Ida[2], T.Kobayashi[2], M.Yoshinuma[2], Y.Nakamura[2], M.Kisaki[2], H.Nakano[2], and C.Moon[2]

[1] *Department of Fusion Science, SOKENDAI (The Graduate University for Advanced Studies), Toki, Gifu 509-5292, Japan*
[2]*National Institute for Fusion Science, Toki, Gifu 509-5292, Japan*

(Presented XXXXX; received XXXXX; accepted XXXXX; published online XXXXX)
(Dates appearing here are provided by the Editorial Office)

Beam Emission Spectroscopy is widely used as local density fluctuation measurements of fusion plasmas. We have installed a BES system in the Large Helical Device (LHD) with radially and poloidally elongated optical configuration to enhance both signal-to-noise ratio and wavenumber sensitivity in radial and poloidal direction. The calculation considering the integral effect of line of sight showed the radially and poloidally elongated sightlines have increased sensitivity compared with the square shaped bundle design of the same sampling area.

I. INTRODUCTION

As a method for a multi channel local measurement of density fluctuations, Beam Emission Spectroscopy (BES)[1] has been widely used in fusion experimental devices[2, 3, 4]. A local density fluctuation diagnostic based upon the BES with radially and poloidally elongated sightlines has been implemented on Large Helical Device (LHD)[5] to investigate the spatiotemporal and spectral characteristics of long wavenumber density fluctuations such as MHD activity. The first application of BES to a helical system resulted in the compact helical system (CHS)[6]. In that system, the simultaneous measurement of the density fluctuations and density gradient was accomplished with the optimized sightlines, which are aligned nearly tangent to the magnetic axis. Based on the achievement in the CHS, a BES system with a sightlines passing through the plasma in the poloidal direction was developed in LHD[7,8].That system have detected medge magnetohydrodynamics (MHD) oscillations and achieved the radial profile of the coherence between the density fluctuation and the magnetic fluctuation. It was found that e-noise in the root mean square value corresponds to around 5% of the dc value of the signal in the detected fluctuation spectrum, and the signal-to-noise ratio had to be improved to measure turbulences. Because of the larger size of the LHD, which has a major radius R of 3.5 m and an averaged minor radius of 0.6 m, the distance from diagnostic ports to the plasma is larger and the solid angle for collecting beam emissions is smaller. Therefore, it is required to increase the sampling area to achieve sufficient detected photon flux and signal-to-noise ratio for fluctuation spectral analysis. In most conventional BES systems, a sampling area is a round shape due to the shape of a fiber or a rectangular shape with bundled fiber image[4,9], leading to almost the same wavenumber sensitivity in two directions on a focal plane. The optical fiber geometry which yields a slit-shaped sampling images in a plasma is applied to the BES system in LHD. The idea of the fiber configuration is

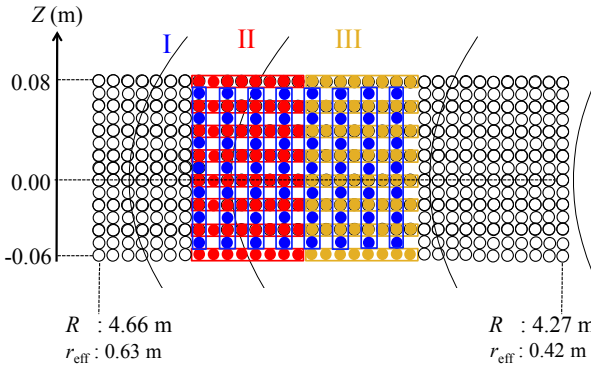

FIG. 1. Fiber image configuration on the poloidal cross section. Each channel of group I (blue circle) consists of 7 fibers making poloidally elongated slit shaped sampling area, while group II and III yield radially elongated sampling area with 8 fibers in each channel. Two types of slits are overlaid in the same area.

that utilizing the fiber bundle design that the images of fibers elongated along radial or polidal direction to achieve both enhance ment of photon flux and good wavenumber resolution in the directions along the narrow sides of the slits. Poloidally elongated sightlines are aligned in the radial direction to investigate the radial profile and propagation characteristic of density fluctuations, and radially elongated sightlines are aligned in the poloidal direction to investigate the poloidal structure of the fluctuations. These slit-shaped sightlines have the advantage that the wavenumber sensitivity is increased in the direction perpendicular to the slit direction. By combining the two sets of the radially and poloidally elongated sightlines in a same sampling area, both radial and poloidal wavenumber sensitivity are improved compared with the conventional square-shaped sightline. This configuration is expected to enable simultaneous measurement of radial

[a)]Contributed paper published as part of the Proceedings of the 21st Topical Conference on High-Temperature Plasma Diagnostics (HTPD 2016) in Madison, Wisconsin, USA.
[b)] ohno.makoto@nifs.ac.jp

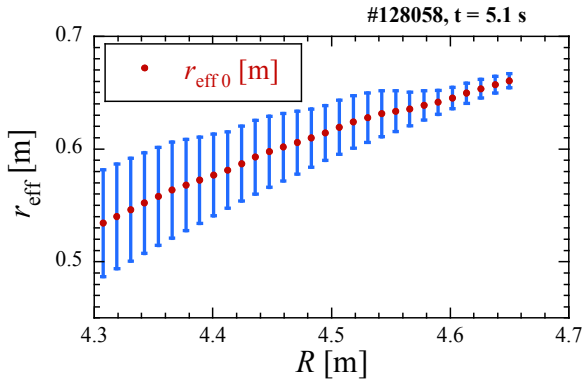

FIG. 2. Contour plot for (a) the multiple value of n_e and n_{beam}, and (b) r_{eff} on the equatorial plane. (c) Evaluation of the location and spatial resolution of lines of sight in the range of $4.30 < R < 4.65$ m.

and poloidal characteristics of the density fluctuation. This article presents the sightline design and the estimated wavenumber sensitivity

II. OPTICAL FIBER BUNDLE DESIGN

As a probe beam, a perpendicularly injected hydrogen heating neutral beam is used, and its accelerating energy is typically 40 keV. The angle between the sight lines and the beam line is ~120° at the edge of the plasma, yielding a Doppler blue shift of ~3.0 nm in the H_α beam emission. Figure 1 shows the fiber image configuration on the poloidal cross section. Each channel consists of 7 (or 8) 400-μm-diam fibers arranged in line along poloidal or radial direction. Each fiber bundle of an array for radial wavenumber measurement images 10 x 130 mm and has a radial spatial separation of 20 mm. Each fiber bundle of an array for poloidal wavenumber measurement images 80 x 10 mm and has a poloidal spatial separation of 20 mm. These two types of arrays are overlaid in the same region to form a lattice-configuration and views 160 x 150 mm in total. The array for radial wavenumber measurement averages the signals for 130 mm in poloidal direction, while that for poloidal wavenumber measurement averages for 80 mm in radial direction. The collected light is transmitted to a spectrometer[10] and is detected simultaneously with the 4 x 8 pixel avalanche photodiode camera with a sampling frequency of 200 kHz.

III. Radial spatial resolution

The images of the light collecting fiber set for viewing perpendicularly injected neutral beam have a spatial width of 1 cm and a spatial pitch of 1 cm on the focal plane. Because of the probe beam width, the sampling volumes of each line of sight pass through several magnetic flux surfaces, and this leads to integration of beam emission across different flux surfaces. Thus, it is essential to estimate this integral effect to evaluate the localization of the measurement. If we define the spatial resolution as the standard deviation in effective minor radius weighted by the

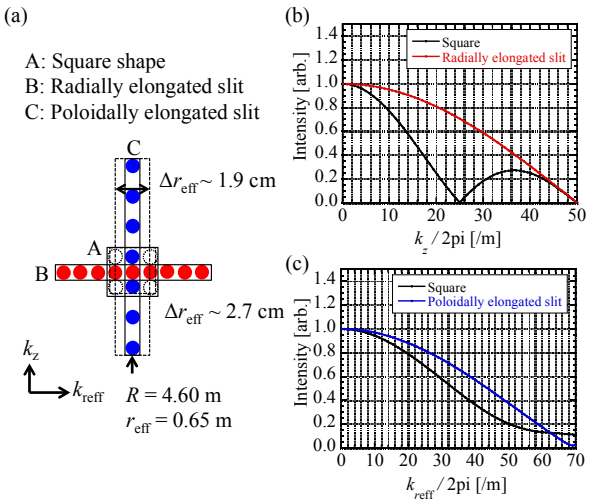

FIG. 3. (a) Three types of fiber bundle design. Comparisons of wavenumber sensitivity for a wave propagating in (b) poloidal direction and (c) radial direction.

multiple value of electron density n_e and beam particle density n_{beam} along each sight line, this is expressed as

$$\Delta r_{\mathrm{reff}} = \sqrt{\int w \times (r_{\mathrm{reff}} - r_{\mathrm{reff}\,0})^2 \, dl}, \tag{1}$$

where, w is defined

$$w = \frac{n_e \times n_{\mathrm{beam}}}{\int n_e \times n_{\mathrm{beam}} \, dl}, , \tag{2}$$

and measurement central position in radial direction $r_{\mathrm{eff}\,0}$ is defined

$$r_{\mathrm{eff}\,0} = \int w \times r_{\mathrm{eff}} \, dl. , \tag{3}$$

The evaluated location for lines of sight in the range of $4.30 < R < 4.65$ m is $0.66 < r_{\mathrm{eff}\,0} < 0.53$ m. The spatial resolution is $2\Delta r_{\mathrm{eff}}$ ~ 0.01 m at the edge and this increases up to ~ 0.10 m. The ratio of the light intensity emitted from the region of $r_{\mathrm{eff}\,0} \pm \Delta r_{\mathrm{eff}}$ to the total light intensity integrated along a sight line is expressed

$$w_0 = \sqrt{\int_{r_{\mathrm{reff}\,0} - \Delta r_{\mathrm{reff}}}^{r_{\mathrm{reff}\,0} + \Delta r_{\mathrm{reff}}} w \, dr_{\mathrm{reff}}}. \tag{4}$$

For the region of $4.30 < R < 4.65$ m, w_0 was estimated ~ 68%. The deviation in r_{eff} of the poloidally elongated slit sight lines in the range of $3.3 < R < 3.6$ m is around 0.01 m for the typical discharges in LHD. This deviation is smaller than the line integral effect.

IV. Wave number sensitivety

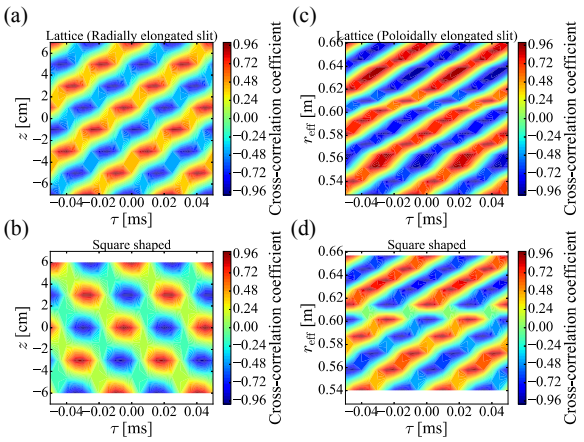

FIG. 4. Contour plots of cross correlation function of the test wave data (f = 20 kHz, $k_{r\mathrm{eff}}/2\pi$ = 20.0 m^{-1}, $k_z/2\pi$ = 18.2 m^{-1}) in poloidal direction detected with (a) radially elongated sightlines (group I in Fig1) and (b) square shaped sightlines, and in radial direction detected with (c) poloidally elongated sightlines (group II) and (d) square shaped sightlines.

Figure 3 (a) shows the shapes of the fiber bundles of square (A), radially elongated slit (B), and poloidally elongated slit (C). The radially location for each bundle types was taken at R=4.60 m (r_{eff} ~ 0.65 m at the intersection of the line of sight and the probe beam center on the equatorial plane). For comparisons of wave number sensitivity among the different types of bundle design, intensity of collected light by using each bundle design was calculated. The sensitivity is taken as a root mean square value of collected wave intensity at each fiber image of the bundle design and normalized with the wave intensity collected with a dot shaped sampling image at the center of the bundle. This calculation is done with consideration of the line integral effect in radial direction (Δr_{eff}), and wave amplitude is weighted with the multiple value of n_e and n_{beam}. The test wave data is a 20 kHz plane wave in (r_{eff}, z) plane with white spectrum of k_z (or $k_{r\mathrm{eff}}$) and $k_{r\mathrm{eff}}$ = 0 (or k_z = 0). Figure 3 (b) shows the poloidal wave number sensitivity for each bundle design. While the poloidal wave number sensitivity of square and poloidally elongated slit drop sharply, the radially elongated slit keeps sensitivity up to $k_z/2\pi$ = 50 m^{-1}, which corresponds to the inverse of the double value of the fiber image diameter. For the wavelengths of which the integer multiple correspond to the length in poloidal direction of the sampling areas, the collected signals are averaged to be zero, and this can be the sensitivity drop. Figure 3 (c) shows the radial wave number sensitivity for each bundle design. Although the sensitivities are almost comparable between the radially elongated sightline and the square shaped sightline because the width of sampling areas in radial direction are almost similar (Δr_{eff} is 1.9 and 2.7, respectively), the poloidally elongated slit has better sensitivity in the range of $0 < k_{r\mathrm{eff}}/2\pi < 60$.

V. Spatiotemporal structure reconstruction

Spatiotemporal structure of fluctuations is determined by a two-point two-time correlation function at a different position. Two-point two-time correlation function can be given by

$$R(x,\tau) = \frac{\left\langle I(x,t) I_{\mathrm{ref}}(t+\tau) \right\rangle}{\sqrt{\left\langle I^2(x,t) \right\rangle} \sqrt{\left\langle I_{\mathrm{ref}}^2(t) \right\rangle}}, \quad (5)$$

where τ is the time lag, $I(x,t)$ is the time series of the channel located at x, $I_{\mathrm{ref}}(t)$ is the time series of the reference channel, and $\langle\ \rangle$ stands for temporal average. Figures 4 (a) and (c) show a contour plot of correlation functions of the test wave data (f = 20 kHz, $k_{r\mathrm{eff}}/2\pi$ = 20.0 m^{-1}, $k_z/2\pi$ = 18.2 m^{-1}) detected with slit-shaped sightlines (group I and III in Fig.1) for poloidal direction and radial direction, respectively. From the slope of the peak in those contour plots, radial and poloidal phase velocity can be estimated (v_r, v_θ) ~ (1.0, 1.1) [km/s], corresponding to the value calculated with wavelength and frequency. Figures 4 (b) and (d) shows the contour plots of cross correlation of the wave sampled with square shaped sightlines. With the reduced number of channels of the square type array compared to the array of radially elongated sightlines and the spatial pitch comparable to the half of the wavelength in this case, the contour of correlation function cannot reconstruct the propagation direction (Fig.4 (c) and (d)).

VI. SUMMARY

We installed the LHD BES system with radially and poloidally elongated sightlines, and have estimated wavenumber sensitivity considering the integral effect of line of sight. We summarized the configuration has the enhanced sensitivity for the poloidal wavenumber and radial wavenumber with radially elongated slit and poloidally elongated slit shaped bundle design compared with the square shaped bundle design of the same sampling area. The systems using the radially and poloidally elongated sightlines configuration will be applied to investigate space correlations in radial/poloidal directions.

ACKNOWLEDGMENTS

The authors would like to thank the LHD Experiment Group for their effort in supporting the experiment in LHD. This work is partly supported by MEXT KAKENHI Grant Number 23246164. This work is also partly supported by the National Institute for Fusion Science grant administrative budget NIFS10ULHH021.

[1]R. J. Fonck, *et al.*, Rev. Sci. Instrum., 61, 3487 (1990).
[2]R. D. Durst, *et al.*, Rev. Sci. Instrum., 63, 4907 (1992).
[3]G. R. McKee, *et al.*, Rev. Sci. Instrum., 70, 913 (1999).
[4]D. R. Smith, *et al.*, Rev. Sci. Instrum., 81, 10D717 (2010).
[5]A. Iiyoshi, *et al.*, Nucl. Fusion, 39, 1245 (1999).
[6]T. Oishi, *et al.*, Rev. Sci. Instrum. 75, 4118 (2004)
[7]T. Oishi, *et al.*, Rev. Sci. Instrum. 81, 10D719 (2010)
[8]S. Kado, *et al.*, Rev. Sci. Instrum. 81, 10D720 (2010)
[9]D. K. Gupta, *et al.*, Rev. Sci. Instrum., 75, 3493 (2004).
[10]M. Yoshinuma, *et al.*, Fusion Sci. Tech., 58, 375 (2010)

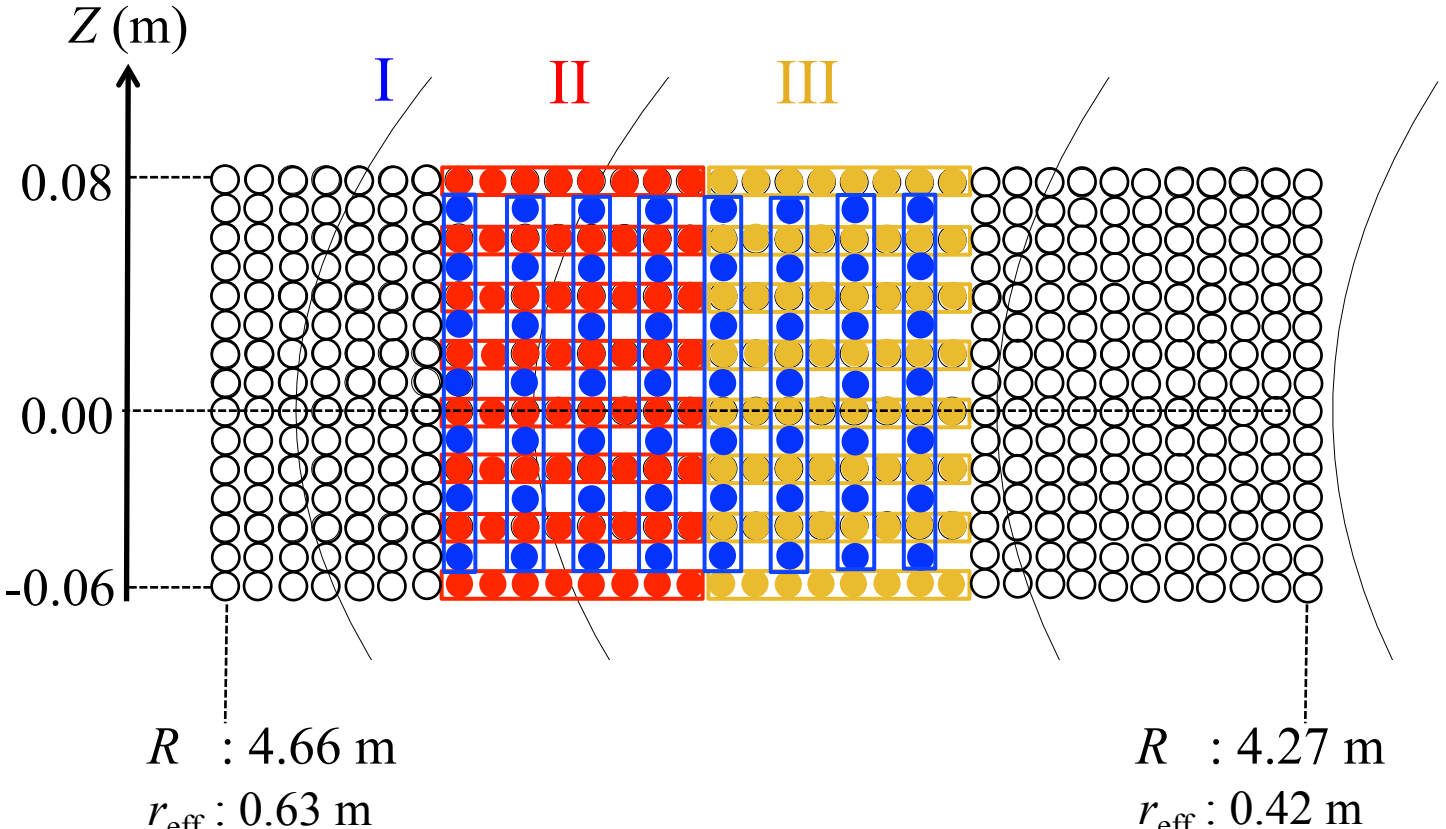
Z (m)
I
II
III
0.08
0.00
-0.06
R : 4.66 m
r_eff : 0.63 m
R : 4.27 m
r_eff : 0.42 m

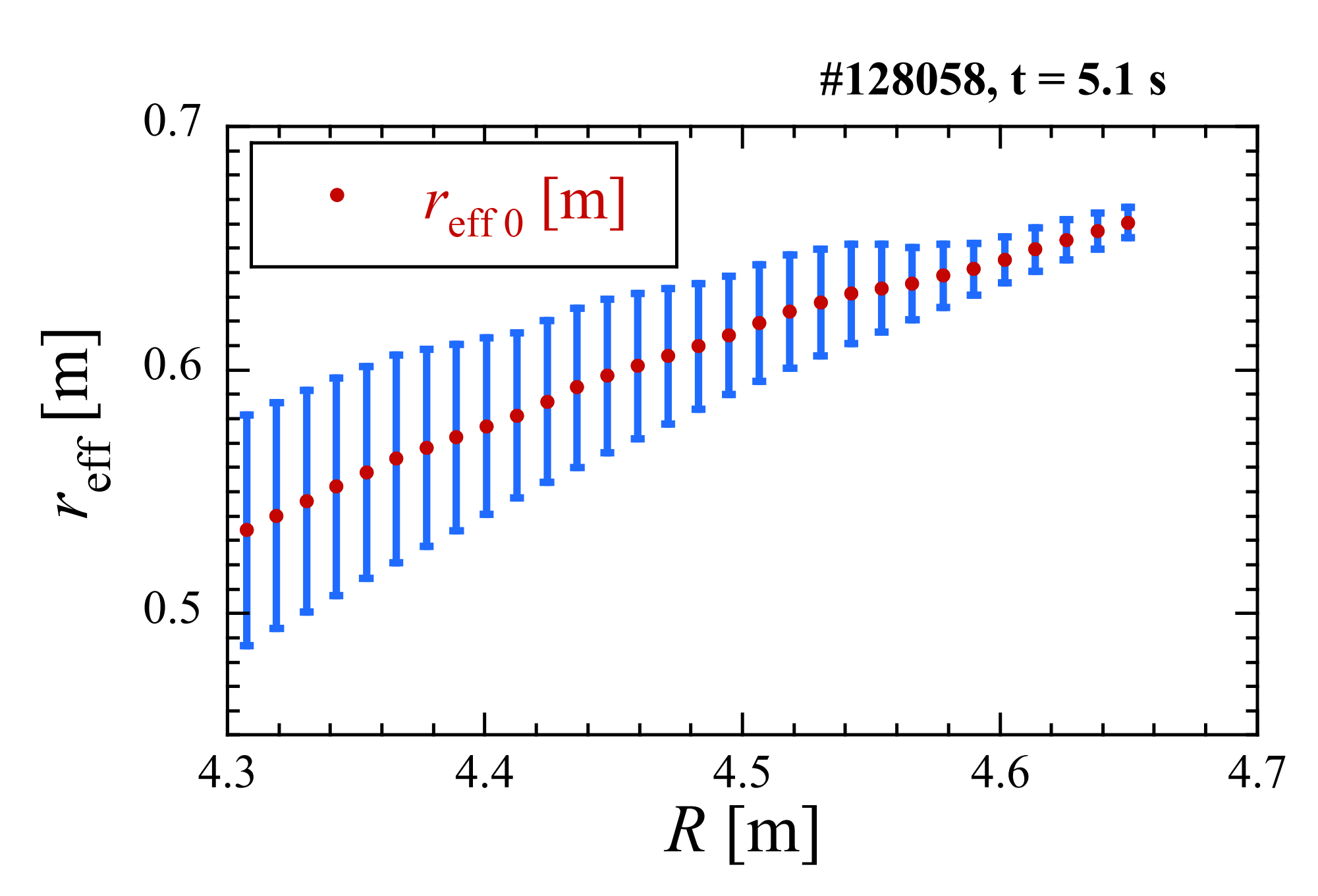
#128058, t = 5.1 s
$r_{\mathrm{eff}\,0}$ [m]
r_{eff} [m]
0.7
0.6
0.5
4.3
4.4
4.5
4.6
4.7
R [m]

(a)

A: Square shape
B: Radially elongated slit
C: Poloidally elongated slit

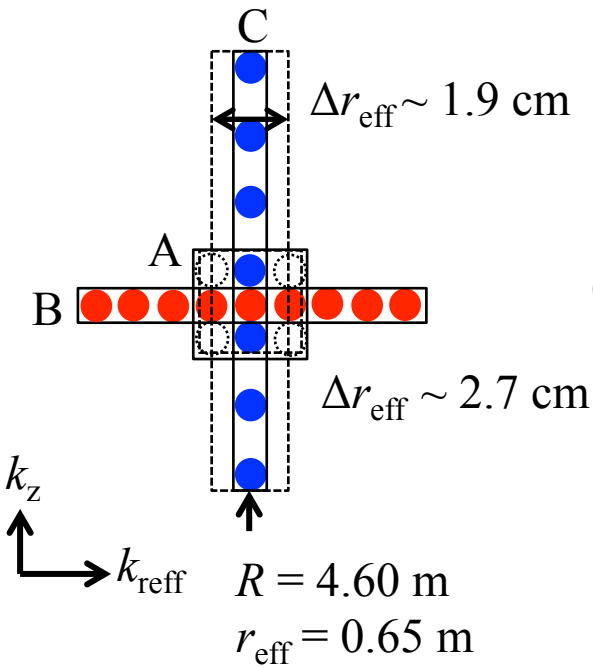

(b)

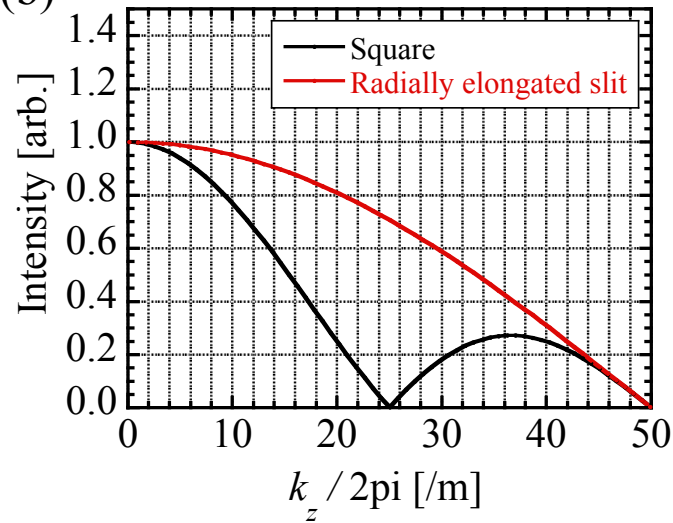

(c)

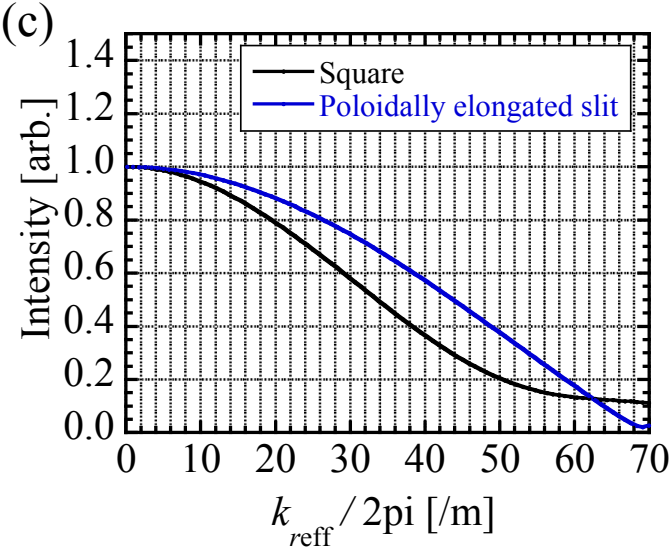

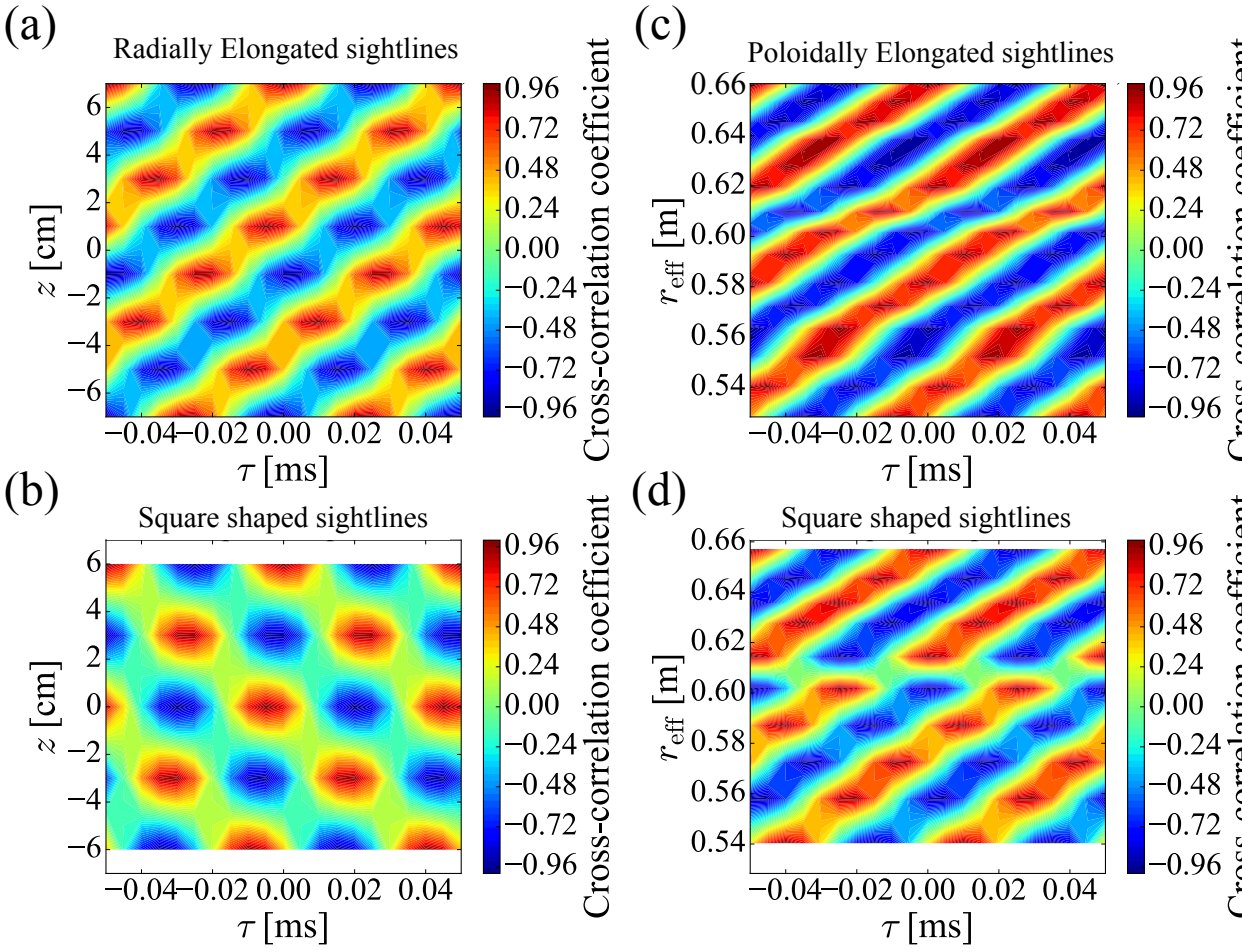
(a)
Radially Elongated sightlines
z [cm]
τ [ms]
Cross-correlation coefficient
(b)
Square shaped sightlines
z [cm]
τ [ms]
Cross-correlation coefficient
(c)
Poloidally Elongated sightlines
r_eff [m]
τ [ms]
Cross-correlation coefficient
(d)
Square shaped sightlines
r_eff [m]
τ [ms]
Cross-correlation coefficient